JCTC Journal of Chemical Theory and Computation

Hierarchical Numerical Solution of Smoluchowski Equations with Rough Potentials

Polina Banushkina and Markus Meuwly*

Department of Chemistry, University of Basel, Klingelbergstrasse 80, 4056 Basel, Switzerland

Received September 1, 2004

Abstract: We present an efficient and numerically robust algorithm to follow diffusive processes on rough potential energy surfaces. The hierarchical nature of the algorithm (hierarchical discrete approximation or HDA) fully explores the fine- and coarse-grained structure of the underlying interaction potential. The present approach does not impose any restriction on the topology of the potential. The hierarchical grid allows to capture the roughness of the potential and achieve significant reduction of computational time using fewer grid points compared to other DA methods. HDA is shown to be accurate and efficient by comparing with results from the conventional DA and from the "mean first passage time" (MFPT) method. Using potential-optimized grids HDA monotonically converges to results from an analytical treatment for a very rough interaction potential (107 minima). Contrary to MFPT the solution from HDA is numerically stable. Because of the hierarchical structure of the method HDA can be extended to multidimensional problems.

I. Introduction

The notion of structured (rough) energy landscapes is an important concept in understanding dynamical processes in complex systems. Examples include, but are not limited to, the folding of proteins[1,2] or the reaction of two end-groups in a polymer or polypeptide chain.[3−5] For most systems exhibiting complex behavior the underlying potential or free energy surface has a hierarchical structure with many local, functionally relevant minima.[6,7] As an example, the motion of a peptide or a protein takes place on an energy landscape characterized by a large number of conformational substates (CS).[8−11] At sufficiently low temperatures the system can be trapped in one of the many, essentially isoenergetic substates. The dynamics on this landscape is governed by the heights of the barriers between the local minima which can be of the order of several kT. An important question concerns the time scales on which an initial population of CSs relaxes toward a steady state which, in the case of a protein, is the native state. For this, one or several progression coordinates are usually defined along which an initial population evolves in space and time.[12]

It is of considerable interest to follow the reaction kinetics governed by this complex, rough potential energy surface. One possibility is to characterize the temporal and spatial relaxation of an initial distribution $p(x, 0)$ to the final, steady-state (equilibrium) distribution $p_{eq}(x)$. To this end the Smoluchowski equation (SE) is solved for the particular potential energy function $V(x)$ or the multidimensional energy landscape (for an illustrative example see Figure 9 in ref 9). Since $V(x)$ may be rough (which implies variations on a short spatial dimension), with functionally relevant local minima, it is important to resolve as many details of $V(x)$ as possible. Under such circumstances the entire morphology of $V(x)$ is important, and averaging over its structural features would alter the predicted dynamics and time scales.

There exist several methods to solve SEs. They include finite-difference schemes in x and t,[12] finite-differences in x with time propagation based on the formal solution of the time-dependent part,[13,14] basis set expansions,[15,16] computer simulations, or path integrals.[15] In the first approach one follows the evolution of $p(x, t)$ using finite difference approximations in x and t. Such an approach (implicit scheme) is based on spatial and temporal discretization with resolution Δx and Δt. Since finding the solution at a later time requires knowledge about the solution of the SE at the

* Corresponding author phone: +41 61 267 3821; fax: +41 61 267 3855; e-mail: m.meuwly@unibas.ch.

10.1021/ct0499480 CCC: $30.25
Published on Web 02/12/2005

previous time steps implicit methods are best suited to investigate fast processes or situations where interconversion barriers are low.[12] The second approach uses the closed form for the probability distribution. This requires the diagonalization of the rate constant matrix constructed on a discrete spatial grid with resolution Δx. With an increasing number of grid points the computational effort significantly increases due to storage requirements and execution time. Both grow exponentially with the number of degrees of freedom. After diagonalization of the rate matrix the time evolution of $p(x, t)$ can be readily evaluated at any given t. One method belonging to the latter class is the discrete approximation (DA). Although the first two methods are conceptually simple and appealing, their applicability to problems with realistic potential energy curves is limited.[17] With an increasing number of intermediate states, Δx must decrease and the number of grid points required increases. Such a procedure becomes impractical for very fine grids since the size of the rate matrix increases with an increasing number of CSs. Basis set expansions suffer from similar limitations and the fact that the required eigenvalues are only known for very simple interaction potentials.[16] The major concern in applying methods based on computer simulations is the reduction of statistical errors. Finally, progress has been made in using path integral techniques although numerically robust results at a reasonable computational effort were limited to smooth one-dimensional potentials.[18,19] Other methods, primarily related to the motion on rough potential energy curves, include approximations based on analytical mean first passage times.[14,17,20] Unfortunately, these approaches are restricted to one-dimensional systems, and generalizations to multidimensional dynamics are difficult and in fact seem not to have been successful so far.[17]

In this work we present a numerically robust and computationally efficient algorithm to solve the SE for rough potentials. The method explores the hierarchical structure of complex energy landscapes for which averaging over the roughness may not be possible. We apply the method to smooth and rough potentials and, if available, compare the results with previously developed methods. The model potentials we investigate include a harmonic potential $V(x) = 1/2\ kx^2$ (H1), a double well potential $V(x) = \cos(3.14(x - 3))$ (A1), a rough one-dimensional potential $V(x) = kx^2/2 + \epsilon(\cos(167x) + \sin(73x))$ (R1) where $k = 19.84$ (kcal/mol)/Å^2, $\epsilon = 0.595$ kcal/mol (see Figure 1) and two-dimensional potentials $V(x, y) = 1/2\ kr^2$ (H2), $V(x, y) = -2\cos(6r) + (\exp(r - 0.7))^2$ (A2), $V(x, y) = 5r^2 + 0.5(\cos(45(r - 0.0655)) + \sin(30(r - 0.0655)))$ (R2), where $r^2 = x^2 + y^2$ and the last is a rough potential.

Each of the potentials relates to different physical situations. H1 is a test potential used in previous work[14] for the motion in a harmonic potential and the problem can be solved analytically, and A1 involves barrier crossing which becomes important for example in chemical reaction dynamics. R1 is a harmonic potential with a rough background, which was previously used and for which an algebraic treatment exists.[14,17] The same physical picture applies to the potentials in two dimensions.

II. Description of the Hierarchical DA Method

In the large-friction limit the Fokker−Planck equation leads to the Smoluchowski equation which, in one spatial dimension x, reads

$$\frac{\partial p(x, t)}{\partial t} = \frac{\partial}{\partial x} D(x) e^{-\beta V(x)} \frac{\partial}{\partial x} [e^{\beta V(x)} p(x, t)] \qquad (1)$$

Here, $D(x)$ is a space-dependent diffusion constant, $V(x)$ is the interaction potential, $\beta = 1/kT$ is the Boltzmann factor and $p(x, t)$ is the space and time-dependent probability distribution. In the following D is taken to be constant, i.e., $D(x) = D = 0.03$Å^2/s. Using finite differences to approximate the derivatives, equation (1) can be recast as a Master equation[13]

$$\frac{\partial p(x_n, t)}{\partial t} = l(n|n+1)p(x_{n+1}, t) + l(n|n-1)p(x_{n-1}, t) - (l(n+1|\ n) + l(n-1|\ n))p(x_n, t) \qquad (2)$$

Here $l\ (n|n \pm 1)$ are the rates to move to the left and to the right from the starting point x_n.

The time evolution of $p(x, t)$ in Equation (1) can be followed numerically whereby the space coordinate is discretized such that the continuous variable x takes discrete values x_n, $n = 1, \ldots, N + 1$. The solution to (1) may be obtained by solving equations (2). In DA the rate coefficient $l(m|n)$ for making a transition $x_n \rightarrow x_m$ is given by

$$l(m|n) = \frac{D(n) + D(m)}{2d^2} \exp\left(-\frac{\beta(V(m) - V(n))}{2}\right)$$

with $d = x_{n+1} - x_n$ (see ref 13).

For rough potentials $V(x)$ the number of grid points n required to resolve the roughness increases rapidly. This leads to large matrices that have to be accurately diagonalized. In the present work we explore the possibility to solve the (SE) on a hierarchy of grids by defining a coarse grid (N) and a subgrid (M) by dividing each interval (x_n, x_{n+1}) into $j = 1, \ldots, M + 1$ points. The mean passage time $\tau(n + 1|n)$ from x_n to x_{n+1} is given by[21]

$$\tau(n+1|n) = \int_0^\infty \sum_{j=1}^{M} p(x_j, t)dt = \int_0^\infty (1 - p(x_{M+1}, t))dt \qquad (3)$$

and the corresponding rate coefficients are $l_{\mathrm{HDA}}(n + 1|n) = 1/\tau(n + 1|n)$. For finding $\vec{p}_{\{M+1\}}(x, t)$ ($\vec{p}_{\{M+1\}}(x, t)$ is the vector of probabilities in points $x_1, \ldots, x_{M+1}$ on each subinterval) we use the DA method, and the solution of (2) can be determined from

$$\vec{p}_{\{M+1\}}(x, t) = U \exp(\vec{\lambda} t) U^{-1} \vec{p}_{\{M+1\}}(x, 0)$$

The elements of matrix U and $\vec{\lambda}$ are the eigenvectors and eigenvalues of the rate matrix, respectively. The boundary conditions on each subinterval are

$$l(1|0) = l(0|1) = 0,$$

$$l\ (M + 2|M + 1) = l(M + 1|M + 2) = 0,$$

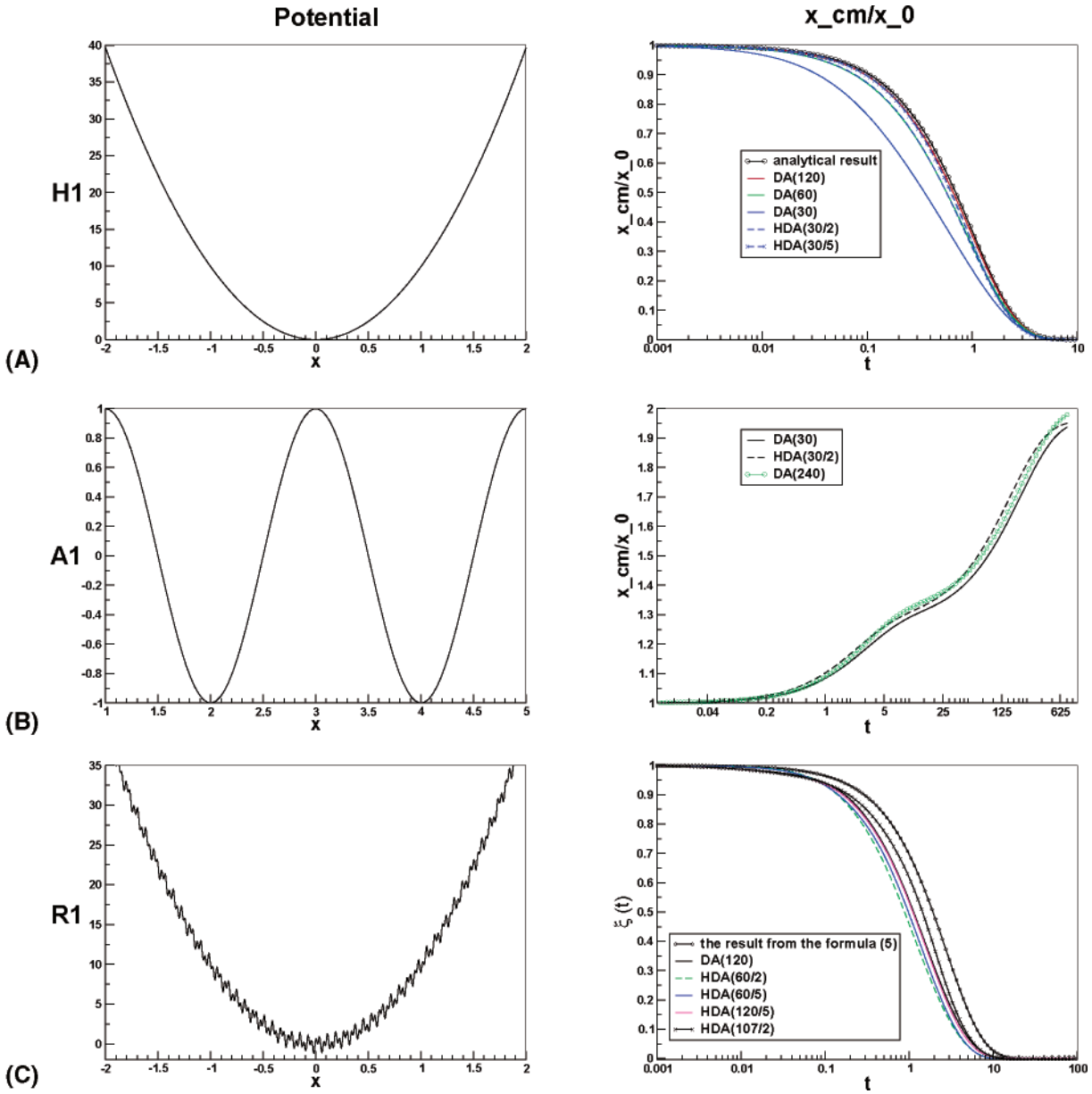

Figure 1. The different 1-d potentials for which the Smoluchowski equation is solved together with the time evolution of the position of the center-of-mass coordinate $x_{cm}(t)/x_0$ as a function of time. (A) For the harmonic potential HDA(30/M) with moderate values of M gives the known analytical result, while for conventional DA 120 points are required. (B) For the double well potential (A1) the initial distribution at $x = 1.5$ relaxes to $x_{cm} = 2$ which is halfway between the two minima of the symmetric potential. HDA(30/2) is found to yield dynamics very close to DA(240). (C) R1 has 107 minima with the global minimum at $x = -0.06$. All methods show decay to the same limiting $\xi(t)$, while their dynamics differs somewhat. Note that t is on a logarithmic scale throughout.

$$l(M|M+1) = 0$$

and the initial condition for the probability distribution is a δ-function at the first point of each subinterval. Taking $\vec{p}_{\{M+1\}}(x, 0) = \{\delta_j p_1\}$ the probability $p(x_{M+1}, t)$ at grid point x_{M+1} (required for $\tau(n+1|n)$) is

$$p(x_{M+1}, t) = \sum_k U_{M+1,k} \exp(\lambda_k t) U^{-1}_{k,1}$$

where $U_{M+1,k}$ and $U^{-1}_{k,1}$ are the $(M+1, k)$-th and $(k, 1)$-th elements of the matrices U and U^{-1}, respectively. Substituting this expression into equation (3) the integral can be evaluated analytically to yield

$$\tau(n+1|n) = \sum_k U_{M+1,k} \frac{1}{\lambda_k} U^{-1}_{k,1}$$

The coefficients $l_{\mathrm{HDA}}(n|n+1)$ are determined from the condition of detailed balance

$$l_{\mathrm{HDA}}(n|n+1) = \frac{l_{\mathrm{HDA}}(n+1|n) p_e(n)}{p_e(n+1)} \qquad (4)$$

where $p_e(x)$ is the Boltzmann equilibrium probability distribution for the potential $V(x)$.

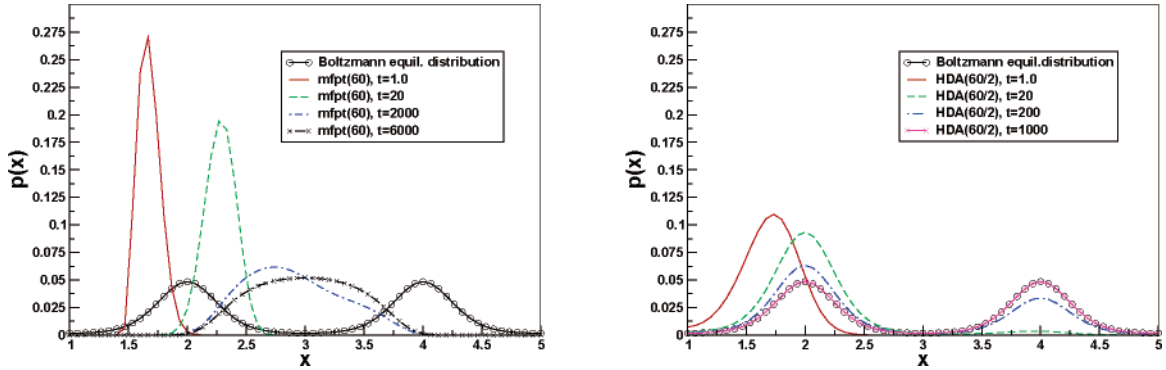

Figure 2. Normalized probability distributions $p(x, t)$ for different times t calculated by the MFPT method (ref 14) and HDA for the A1 potential. For both cases the stationary Boltzmann equilibrium distribution $p_e(x)$ is also given. As shown $p(x, t)$ from MFPT(60) does not converge to $p_e(x)$, while the distribution from HDA(60/2) does.

III. Results

In all cases reflecting boundary conditions are used for the coarse grid N. The left and right boundaries are $[-2,2]$ for H1 and R1 and [1.5] for A1. For the 2-d calculations they are a square on $[-1,1]$ in both dimensions for H2 and R2 and $[-1.5,1.5]$ in both dimensions for A2. In the following we will use the notation DA(N) for a DA calculation with N spatial grid points and HDA(N/M) for an HDA calculation with N coarse grid points and M points in the subgrid.

1-Dimensional Potentials. A convenient measure for the relaxation from the initial distribution $p(x, 0)$ is to follow the center-of-mass $\xi(t) = x_{cm}(t)/x_0$ of the distribution, where $p(x, 0)$ is the initial distribution which is a δ-function located at the nearest grid point to $x_0 = -1.5$, 1.5 and -1.0 for cases H1, A1, and R1, respectively. In Figure 1 the time evolution of $\xi(t)$ of the distribution function calculated by DA and HDA is shown for the three different 1-d potentials.

For the harmonic potential H1, DA(30) is far from the analytical result, while HDA(30/2) and HDA(30/5) rapidly approach the exact $\xi(t)$. Convergence toward the known result is much slower for conventional DA and only achieved for DA(120). The relative speedup of HDA compared to conventional DA is about a factor of 50.

For the anharmonic potential (A1) DA(30) yields a somewhat slower decay toward the minimum than HDA(30/2) which gives $\xi(t)$ in close agreement to the one calculated with DA(240) (see Figure 1B). It is only in the very long time limit ($t > 500$s) that $\xi(t)$ from HDA(30/2) and DA-(240) start to show appreciable differences. Calculations with DA(1000) give $\xi(t)$ marginally different from DA(240). Using MFPT(60), the method from ref 14, $\xi(t)$ converged to the correct long-time limit ($\xi(t) = 2$). However, the overall behavior of $\xi(t)$ was different from the ones shown in Figure 1B using either DA or HDA. To understand this further $p(x, t)$ at different time t was calculated and is shown in Figure 2. They were calculated with MFPT(60) (the method from ref 14) and HDA(60/2). Using the MFPT-method $p(x, t)$ has reached the equilibrium distribution $p_e(x)$ for $t > 6000$ while $p(x, t)$ from HDA is stationary after $t > 1000$ which means that the two methods yield different dynamics. As is shown, $p(x, t \rightarrow \infty)$ from MFPT does not converge to the known $p_e(x)$ although $\xi(t)$ reaches the correct long time limit. One possible explanation is that the rate coefficients used in the MFPT method do not explicitly fulfill the condition for detailed balance (equation (4)).

Besides the motion in a harmonic and bistable potential, energy profiles with roughness are of interest. Previous work[14,17] has established that the average position $x_{cm}(t)$ of the particle diffusing on the R1 potential (roughness with a harmonic background) can be found from the analytical formula for H1 with a modified effective diffusion coefficient D'

$$x_{cm}(t) = x_0 \exp(-k\beta D' t) \tag{5}$$

where $D' = D \exp[-(\epsilon/k_\beta T)^2]$. Generalizations to potentials with different than a harmonic background apparently have not yet been discussed in the literature. The R1 potential has 107 local minima on the interval $[-2,2]$. In Figure 1C the results from DA, HDA and the result from formula (5) are shown. The latter result is taken as the reference. One possible (but somewhat arbitrary) measure to compare the different methods is the time τ at which $\xi(t)$ has reached its half time value $\xi(t) = 0.5$. For the result from formula (5) $\tau = 1.9$ while for DA(120) $\tau = 1.2$. Using HDA(60/2) and HDA(60/5) gives faster kinetics (with $\tau = 0.89$ and $\tau = 1.07$, respectively). It is interesting to note that with increasing M at constant N the solution from HDA systematically improves and converges. However, with equidistant points it was not possible to approach the result from formula (5).

With DA and HDA it is also possible to use nonequidistant grids. Locating the x_i at the local minima of R1, i.e., $N = 107$, the $\xi(t)$ from HDA(107/2) is closer to the $\xi(t)$ calculated from formula (5) than $\xi(t)$ from DA(120) and for HDA(120/5) and $\xi(t) = 0.5$ was reached at $\tau = 1.52$. Previously it was shown that the MFPT method gives essentially exact results even with $N = 30$.[14] However, by increasing N to $N = 35$ we found that MFPT is unstable. For the R1 potential $\xi(t)$ should be strictly bounded ($1 \leq \xi(t) \leq 0$, see Figure 1C). However, for $N > 30$ $\xi(t)$ from MFPT takes values outside this interval. Contrary to that, HDA monotonically converges for fixed N and increasing M.

2-Dimensional Potentials. In 2 spatial dimensions the application of conventional DA already becomes prohibitive. The maximum number of intervals possible was $N = 50$ in each dimension. Here we used the same number of intervals

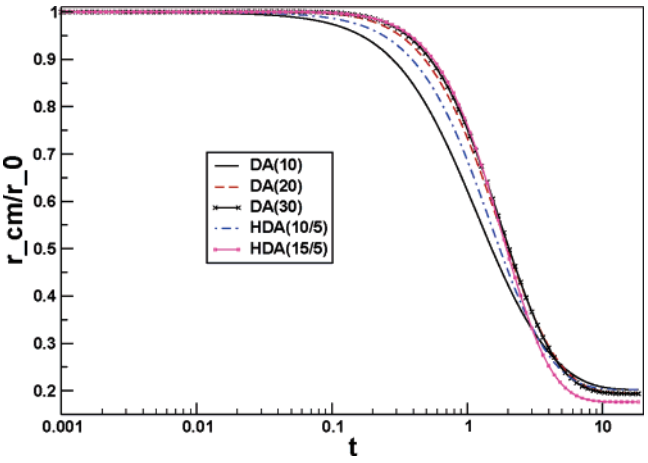

Figure 3. The mean radius $\xi(t) = (r_{cm}(t)/r_0)$ of $p(x, y, t)$ is plotted as a function of time for the H2 potential. The limiting values for $\xi(t \rightarrow \infty)$ are different because the locations of the grid points differ for N even and N odd. The dynamics for DA(30) and HDA(15/5) are virtually identical. Computing times, however, differ by a factor of 30 (see text). The time t is on a logarithmic scale.

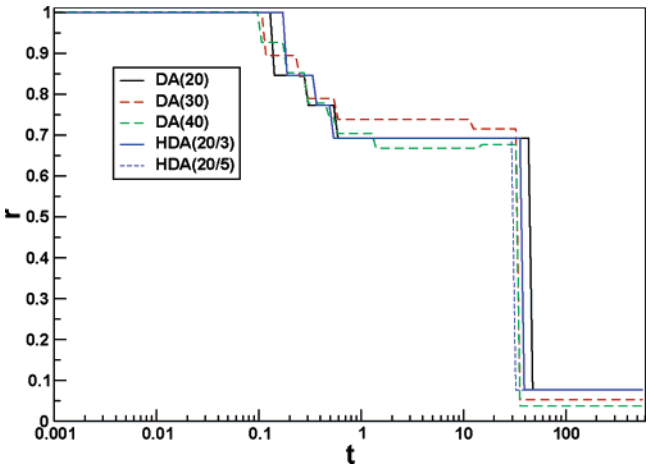

Figure 4. Position of the maximum $p_{max}(x, y, t)$ relative to its initial position $p(x_0, y_0, 0)$ as a function of time for the A2 potential. Results from calculations with different grid sizes for DA and HDA are shown. The long-time value of $g(t)$ depends on the number of grid points.

in the x and y direction. However, depending upon the topology of $V(x, y)$ this might not be the optimal choice. There are different possible measures how to compare the relaxation from $p(x, y, 0)$ to $p_e(x, y)$ ($p(x, y, 0)$ is a δ-function located at the nearest grid point to $(x_0, y_0) = (-0.8, -0.8)$ for H2; $(-1, -1)$ for A2 and $(-0.9, -0.9)$ for R2, respectively). One possibility is to follow the mean value of the length of the radius vector of the distribution $p(x, y, t)$. The radius vector is measured from the point (0,0) to the point (x_i, y_j), and we define the mean radius as $r_m(t) = \sum_{i,j=1}^{N+1} r(x_i, y_j)p(x_i, y_j, t)$. To compare the results of the DA and HDA method on the H2 potential the time evolution of the value $\xi(t) = r_m(t)/r_0$ is followed, where $r_0 = \sqrt{x_0^2+y_0^2}$. Figure 3 shows that $\xi(t)$ from HDA(10/5) is close to DA(20) and HDA(15/5) approaches the result from DA(30). With HDA(20/5) (results not shown) $\xi(t)$ is virtually identical to the one from DA(30). The different long-time value for $\xi(t \rightarrow \infty)$ for DA(30) and HDA(15/5) is a consequence of the different locations of the grid points. To calculate the decay from the initial distribution $p(x, y, t)$ was followed for 80 time steps. The computing times were 0.3, 2, 5 and 77 min for HDA(10/5), HDA(15/5), DA(20) and DA(30), respectively, on an AMD 1666 MHz workstation.

For the A2 potential $\xi(t) = r_m(t)/r_0$ turned out to be not a suitable measure. We found that the time dependence of $\xi(t)$ depends on the location of the grid points. Even small differences in the values of the probability distribution calculated by DA and HDA at the same time lead to considerable changes in $\xi(t)$. It is more useful to monitor the position of the maximum $p_{max}(x, y, t)$ relative to its initial position $p(x_0, y_0, 0)$, i.e., the time evolution of $g(t) = r_{max}(t)/r_0$, where $r_{max}(t)$ and r_0 are the distances of $p_{max}(x, y, t)$ and $p(x_0, y_0, 0)$ from the point (0,0), respectively. The function $g(t)$ is not continuous since the maximum can be localized for extended periods of time on the same grid point. Initially, $p_{max}(x, y, t)$ is in (x_0, y_0). Although $p(x, y, t)$ changes in time, the position of the maximum resides in (x_0, y_0) up to $t = 0.1$. This can be understood from the shape of A2 which is a rotated double well potential around (0,0). At early times $p(x, y, t)$ spreads within the outer rim and up to $t = 0.7$ the position of $p_{max}(x, y, t)$ changes marginally. Between $t = 1$ and $t = 20$ the global minimum is populated, which, after about $t = 30$ becomes more populated than any other region. For DA(20) the time t_{lim} after which $g(t)$ stabilizes (see Figure 4) is reached significantly later ($t_{lim} = 49$) than for DA(30) and DA(40) for which $t_{lim} = 35$ (Figure 4). For HDA(20/3) and HDA(20/5) t_{lim} are 38 and 33.5, respectively, close to the results from DA(30) and DA(40). However, the CPU time for DA(30) is 110 min compared to 6 min for HDA(20/3). Again, the limiting value $g(t \rightarrow \infty)$ depends on the grid spacing. This is why the curves in Figure 4 do not converge to the same value for $g(t)$. As in the case of (H1) and (A1) rapid convergence of the observables for increasing M at fixed N is found.

Since for A2 the distribution of the grid points influences the analysis of how $p(x, y, t)$ relaxes this is even more so for the rough R2 potential. The R2 potential has about 160 local minima. Grids with $N = 30, 40, 50$ have their points in different places, and the measure for how $p(x, y, t)$ evolves in time will depend on this (see also discussion of Figure 4). To avoid this problem for R2 we follow the distribution of the first passage times for the system to reach the minimum starting from the initial distribution. The value $p(t)$ is the probability that the first passage time to reach the minimum is t. The distribution $p(t)$ was calculated for HDA(20/4), HDA(30/4), HDA(40/4), HDA(50/4). As is shown in Figure 5 HDA(30/4) gives the same result as HDA(50/4). This is in line with the observations for R1 where we also found that at fixed M the results from HDA rapidly converge for increasing N (compare HDA(60/5) and HDA(120/5) in Figure 1). However, for this potential we found that increasing the number of inner points M does not change the behavior of $p(t)$.

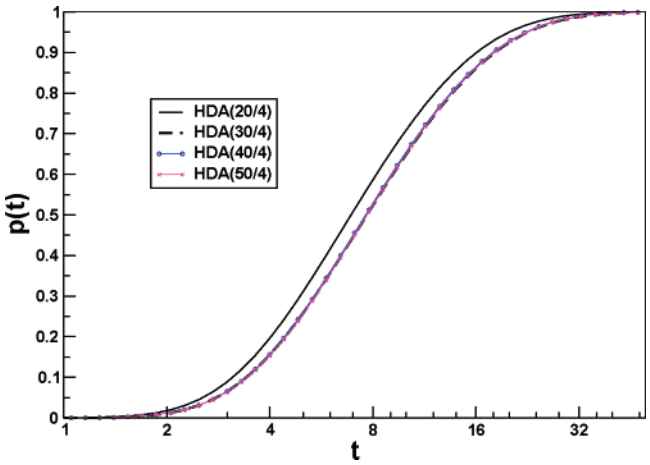

Figure 5. Temporal evolution of the distribution $p(t)$ of the first passage times in the R2 potential. For given $M = 4$ convergence of $p(t)$ is reached at $N = 30$.

IV. Discussion and Conclusion

Numerical approaches to solve the SE for a general form of the (rough) potential energy surface are a useful complement to analytical formulas to treat barrier crossing and escape processes. This is mainly because analytical work gives exact results only for limiting cases such as high barriers, weak or large friction, or particular forms for the potential.[22] In this work a numerically stable and computationally efficient algorithm to solve the SE for rough potential energy surfaces, where averaging over the coarse- and fine-grained structure of the potential is not possible, has been developed. Such approaches become increasingly important since free energy simulations are possible routinely and will provide free energy surfaces in several dimensions.[23,24] To demonstrate its accuracy the SE was first solved for a number of test potentials for which other solution strategies have been presented in the literature. For smooth 1d potentials, results from analytical solutions and the MFPT method serve as comparison for the HDA method. Application of DA and HDA to an anharmonic and rough 1d potential showed that the MFPT method[14] has to be used with circumspection. For A1 MFPT does not converge to the known Boltzmann distribution at long times, and for R1 MFPT(30) yields essentially exact results while MFPT(35) is unstable. For some cases considered here, MFPT appears not always to converge properly upon increasing the number of grid points N as expected. It is interesting to note that a previous study[16] employed 301 grid points to numerically solve the Smoluchowski equation for a 1d, symmetric bistable potential. Here, a similar number of grid points was deemed sufficient (DA(240) for potential A1) to reach convergence, while HDA(30/2) yields dynamics very similar to DA(240) at much reduced computational cost (eigenvalues of a 30×30 instead of a 240×240 matrix). It is clear that in higher dimensions the DA formulation of this problem is computationally intractable (see discussion of A2 potential). An important advantage of HDA for rough potentials is that the method converges monotonically for given N and increasing M. HDA calculations on the very rough R1 potential (107 minima) using a nonuniform, potential-adapted grid leads to kinetics similar to the one based on the approach by Zwanzig where the roughness is treated as a modified diffusion constant.[17] Further exploration of how to optimally place the grid points for more rapid convergence is worthwhile in particular for problems in more than 1 dimension.

Applying a hierarchical separation considerably speeds up calculations while retaining accuracy. In 2 dimensions HDA scales as $(M)^3 \times (N_1)^2 + (N_1^2)^3$, while conventional DA scales as $(N_2^2)^3$ with $N_1 \ll N_2$. Because M is considerably smaller than N_1 there is an appreciable net overall speedup. For example HDA(15/5) gives the same results at 30 times less CPU time than DA(30) for the 2-dimensional harmonic potential (H2). Exploring the hierarchical structure of the potential or free energy landscape is essential for cases where the many local minima correspond to functional states of a system. Smoothing such a potential is not possible (as would be for noise) since this eliminates important physically, chemically and biologically relevant information. Most numerical and analytical approaches currently available have not yet been applied to this class of potentials.

In summary, HDA is a computationally efficient and numerically robust method for rough potentials. Since HDA can be applied recursively still finer subgrids can be used. This together with more sophisticated ways to place the grid points open possibilities to follow the temporal evolution of the dynamics on rough potentials in more than 2 dimension. Given the impediments for other approaches such as storage limitations (basis set expansions), convergence issues (path integral methods) and reduction of statistical errors (computer simulations)[16,18,19] HDA provides an attractive alternative for approximate solutions of Smoluchowski equations for multidimensional systems involving rough interaction potentials. The applicability of HDA to more general formulations of diffusive motion is currently explored.

Acknowledgment. The authors acknowledge financial support from the Schweizerischer Nationalfonds. M.M. is grateful for the award of a Förderungsprofessur. Comments on the manuscript from Dr. S. Krivov, Prof. J. D. Doll, Prof. T. Kiefhaber, and Dr. R. Bemish are gratefully acknowledged.

References

(1) Socci, N.; Onuchic, J.; Wolynes, P. Diffusive dynamics of the reaction coordinate for protein folding funnels. *J. Chem. Phys.* **1996**, *104*, 5860.

(2) Yang, W. Y.; Gruebele, M. Detection-dependent kinetics as a probe of folding landscape microstructure. *J. Am. Chem. Soc.* **2004**, *126*, 7758.

(3) Wilemski, G.; Fixman, M. Diffusion-controlled interachain reactions of polymers. 1. *Theory J. Chem. Phys.* **1974**, *60*, 866.

(4) Krieger, F.; Fierz, B.; Bieri, O.; Drewello, M.; Kiefhaber, T. Dynamics of Unfolded Polypeptide Chains as Model for the Earliest Steps in Protein Folding. *J. Mol. Biol.* **2003**, *332*, 265.

(5) Wang, X. J.; Nau, W. Kinetics of end-to-end collision in short single-stranded nucleic acids. *J. Am. Chem. Soc.* **2004**, *126*, 808.

(6) Jensen, M.; Park, S.; Tajkhorshid, E.; Schulten, K. Energetics of glycerol Energetics of glycerol conduction through aquaglyseroporin GlpF. *Proc. Natl. Acad. Sci.* **2002**, *99*, 6731.

(7) Krivov, S.; Chekmarev, S.; Karplus, M. Potential energy surface and conformational transitions in biomolecules: a successive confinement approach applied to a solvated tetrapeptide. *Phys. Rev. Lett.* **2002**, *88*, 038101.

(8) Austin, R. H.; Beeson, K. W.; Eisenstein, L.; Frauenfelder, H.; Gunsalus, I. C. Dynamics of ligand-binding to myoglobin. *Biochem.* **1975**, *14*, 5355.

(9) Dobson, C. M. Sali, A.; Karplus, M. Protein Folding: A Perspective from Theory and Experiment. *Angew. Chem., Int. Ed*. **1998**, *37*, 868.

(10) Becker, O. M.; Karplus, M. The topology of multidimensional potential energy surfaces: Theory and application to peptide structure and kinetics. *J. Phys. Chem.* **1997**, *106*, 1495.

(11) Wagner, C.; Kiefhaber, T. Intermediates can accelerate protein folding. *Proc. Natl. Acad. Sci.* **1999**, *96*, 6716.

(12) Jun, B.; Weaver, D. One-dimensional potential barrier model of protein folding with intermediates. *J. Chem. Phys.* **2002**, *116*, 418.

(13) Bicout, D. J.; Szabo, A. Electron-transfer reaction dynamics in non-Debye solvents. *J. Chem. Phys.* **1998**, *109*, 2325.

(14) Ansari, A. Mean first passage time solution of the Smoluchowski equation: Application to relaxation dynamics in myoglobin. *J. Chem. Phys.* **2000**, *112*, 2516.

(15) Risken, H. *The Fokker−Planck equation*. Springer, Berlin, Heidelberg, New York, 1989.

(16) Dunkel, R.; Ebeling, W.; Schimansky-Geier, L.; Hänggi, P. Kramers problem in evolutionary strategies. *Phys. Rev. E* **2003**, *67*, 061118.

(17) Zwanzig, R. Diffusion in a rough potential. *Proc. Natl. Acad. Sci.* **1988**, *85*, 2029.

(18) Drozdov, A. N.; Talkner, P. Path integrals for Fokker−Planck dynamics with singular diffusion: Accurate factorization for the time evolution operator. *J. Chem. Phys.* **1998**, *109*, 2080.

(19) Drozdov, A. N.; Hayashi, S. Self-similar renormalization approach to barrier crossing processes. *Phys. Rev. E* **1999**, *60*, 3804.

(20) Goychuk, I.; Hänggi, P. Ion channel gating: A first-passage time analysis of the Kramers type. *Proc. Natl. Acad. Sci.* **2002**, *99*, 3552.

(21) Szabo, A.; Schulten, K.; Schulten, Z. 1st passage time approach to diffusion controlled reactions. *J. Chem. Phys.* **1980**, *72*, 4350.

(22) Hänggi, P.; Talkner, P.; Borkovec, M. Reaction Rate Theory: 50 years after Kramers. *Rev. Mod. Phys.* **1990**, *62*, 251.

(23) Simonson, T.; Archontis, G.; Karplus, M. Free energy simulation come of age: Protein−ligand recognition. *Acc. Chem. Res.* **2002**, *35*, 430.

(24) Ulmschneider, J. P.; Jorgensen, W. L. Polypeptide folding using Monte Carlo sampling, concerted rotation, and continuum solvation. *J. Am. Chem. Soc.* **2004**, *126*, 1849.

CT0499480